Title

Cardiolipin Remodeling Defects Impair Mitochondrial Architecture and Function in a Murine Model of Barth Syndrome Cardiomyopathy

Journal

Circulation Heart Failure, 14(6)

ISSN

1941-3289

Authors

Zhu, Siting

Chen, Ze'e

Zhu, Mason

et al.

Publication Date

2021-06-01

DOI

10.1161/circheartfailure.121.008289

Peer reviewed

Published in final edited form as:

Circ Heart Fail. 2021 June ; 14(6): e008289. doi:10.1161/CIRCHEARTFAILURE.121.008289.

Cardiolipin remodeling defects impair mitochondrial architecture and function in a murine model of Barth syndrome cardiomyopathy

Siting Zhu, BS[#1,2], **Ze'e Chen, PhD**[#1,2], **Mason Zhu, MS**[1], **Ying Shen, PhD**[3], **Leonardo J Leon, PhD**[4], **Liguo Chi, PhD**[4], **Simone Spinozzi, PhD**[1], **Changming Tan, MD, PhD**[1,5], **Yusu Gu, MD**[1], **Anh Nguyen**[1], **Yi Zhou, PhD**[6], **Wei Feng, PhD**[1], **Frédéric M Vaz, PhD**[7,8], **Xiaohong Wang, PhD**[9], **Asa B Gustafsson, PhD**[4,10], **Sylvia M Evans, PhD**[1,4,10], **Ouyang Kunfu, PhD**[2,*], **Xi Fang, PhD**[1,*]

[1]Department of Medicine, University of California, San Diego, La Jolla, California, USA. [2]Department of Cardiovascular Surgery, Peking University Shenzhen Hospital, School of Chemical Biology and Biotechnology, State Key Laboratory of Chemical Oncogenomics, Peking University Shenzhen Graduate School, Shenzhen, China. [3]Department of General, Visceral and Transplantation Surgery, University Hospital Heidelberg, University Heidelberg, Im Neuenheimer Feld 110, 69120 Heidelberg, Germany. [4]Department of Pharmacology, University of California, San Diego, La Jolla, California, USA. [5]Department of Cardiovascular Surgery, The Second Xiangya Hospital, Central South University, Changsha, Hunan, China. [6]Department of Molecular Biology, University of California, San Diego, La Jolla, California, USA. [7]Laboratory Genetic Metabolic Diseases, Amsterdam UMC, University of Amsterdam, Departments of Clinical Chemistry and Pediatrics, Amsterdam Gastroenterology Endocrinology Metabolism, Meibergdreef 9, 1105 AZ Amsterdam, The Netherlands, [8]Core Facility Metabolomics, Amsterdam UMC. [9]Department of Pharmacology and Tianjin Key Laboratory of Inflammation Biology, School of Basic Medical Sciences, Tianjin Medical University, 300070, Tianjin, China. [10]Skaggs School of Pharmacy and Pharmaceutical Sciences, University of California, San Diego, La Jolla, California, USA.

[#] These authors contributed equally to this work.

Abstract

Background: Cardiomyopathy is a major clinical feature in Barth syndrome (BTHS), an X-linked mitochondrial lipid disorder caused by mutations in *Tafazzin* (*TAZ*), encoding a mitochondrial acyltransferase required for cardiolipin (CL) remodeling. Despite recent description of a mouse model of BTHS cardiomyopathy, an in-depth analysis of specific lipid abnormalities and mitochondrial form and function in an *in vivo* BTHS cardiomyopathy model are lacking.

[*]Corresponding author: Xi Fang, PhD, Assistant Professor of Medicine, University of California, San Diego, School of Medicine, 9500 Gilman Drive, La Jolla, CA 92093-0613, Phone: 858-246-4637; xifang@ucsd.edu, Ouyang Kunfu, PhD, Professor of Cardiovascular Surgery, Peking University Shenzhen Hospital, Department of Cardiovascular Surgery, 1120 Lianhua Lu, Futian District, Shenzhen, Guangdong, China, Phone: +86-755-2650-6501; ouyang_kunfu@pku.edu.cn.

Methods: We performed in depth assessment of cardiac function, CL species profiles, and mitochondrial structure and function in our newly generated *Taz* cardiomyocyte-specific knockout (cKO) mice and Cre negative control mice (n≥3 per group).

Results: *Taz* cKO mice recapitulate typical features of BTHS and mitochondrial cardiomyopathy. Fewer than 5% of cKO mice exhibited lethality prior to 2 months of age, with significantly enlarged hearts. 81.8% of cKOs displayed ventricular dilation at 16-weeks of age, and survived until 50-weeks of age. Full parameter analysis of cardiac CL profiles demonstrated lower total CL concentration, abnormal CL fatty acyl composition, and elevated MLCL to CL ratios in Taz cKO, relative to controls. MICOS and F1F0-ATP synthase complexes, required for cristae morphogenesis, were abnormal, resulting in "onion-shaped" mitochondria. Organization of high molecular weight respiratory chain supercomplexes was also impaired. In keeping with observed mitochondrial abnormalities, seahorse experiments demonstrated impaired mitochondrial respiration capacity.

Conclusion: Our mouse model mirrors multiple physiological and biochemical aspects of BTHS cardiomyopathy. Our results give important insights into the underlying etiology of BTHS cardiomyopathy, and provide a framework for testing therapeutic approaches to BTHS cardiomyopathy, and/or other mitochondrial-related cardiomyopathies.

Keywords

Barth syndrome; *Tafazzin*; cardiolipin; mitochondrial cardiomyopathy

Introduction

Barth syndrome (BTHS) is an X-linked mitochondrial myopathy. Individuals with BTHS present cardiomyopathy, skeletal muscle weakness, neutropenia, and growth retardation[1]. Cardiomyopathy is the major clinical feature in BTHS[1–3]. Heart biopsies from transplant patients have revealed mitochondrial malformations, including abnormal mitochondrial size, disorganized distribution, and abnormal cristae[1, 2], representing key features of mitochondrial cardiomyopathy.

BTHS is caused by mutations in *Tafazzin* (*TAZ*, also known as *G4.5*)[2]. More than 160 pathogenic mutations in *TAZ* have been reported to cause[2]. These mutations are spread across all 11 exons of TAZ, resulting in complete absence or decreased levels of TAZ protein, or loss of TAZ protein function[2]. TAZ is highly expressed in cardiac and skeletal muscle, and functions as a mitochondrial phospholipid-lysophospholipid acyltransferase, involved in the remodeling/maturation of cardiolipin (CL)[2]. CL is essential for numerous mitochondrial structure and functions[2], including bioenergetics, membrane architecture and organization, fusion and fission, and mitophagy, as well as regulation of apoptosis. The importance of TAZ-mediated CL remodeling in maintaining mitochondrial homeostasis and cardiovascular health is underscored by BTHS[2]. Moreover, abnormal CL metabolism is also linked to other forms of heart disease, myocardial ischemia-reperfusion injury[4–6] and heart failure[7, 8]. However, little is known as to detailed molecular mechanisms by which *TAZ* deficiency and consequent CL abnormalities lead to cardiomyopathy.

CL is composed of a glycerol head group and two phosphatidylglycerol backbones bound by four fatty acyl chains[2]. In mammalian heart, the fatty acyl chain composition of mature CL is dominated by linoleic acid (C18:2)[2]. *De novo* synthesis of CL occurs exclusively in the inner mitochondrial membrane (IMM), producing a nascent form of CL, which contains a mixture of fatty acyl chains that differ in length and saturation[2]. To achieve a final symmetric acyl composition (eg. C18:2 in the heart), nascent CL undergoes an extensive remodeling process by deacylation to monolyso-CL (MLCL), and subsequent reacylation, catalyzed by acyltransferases[2]. TAZ is a major acyltransferase in CL remodeling[9, 10]. Mutations in *TAZ* cause inefficient transacylation, resulting in decreased amounts of mature CL. The preserved deacylation of nascent CL leads to accumulation of MLCL. These defects are manifested in BTHS patients by a low total CL concentration, abnormal CL fatty acyl composition, and elevated MLCL to CL ratios[11].

Owing to difficulties in generating a *Taz* knockout mouse model, since BTHS was first described in 1983[1], the majority of studies have utilized non-mammalian organisms (Yeast[12–14], Drosophila[15, 16], Zebrafish[17]), cultured cells[11, 18–20], or a short hairpin RNA *Taz* knockdown mouse[21–24]. Studies in *Taz* knockdown mouse models have resulted in variable phenotypes[21–24], with most studies showing a relatively mild disease phenotype[21–23], while one report showed striking cardiac dysfunction at embryonic and neonatal stages[24]. Although a very recent study reported that deletion of Taz in cardiomyocytes results in perturbed MLCL/CL ratio and cardiac dysfunction[25], no experiments were performed to address absolute levels of each CL lipid species and their side chain composition, which may affect disease etiology. Likewise, understanding consequences of TAZ loss on mitochondrial form and function will be key to understanding disease etiology, yet an in-depth analysis has not yet been performed in an *in vivo* model of BTHS. Here, we have performed a detailed functional, biochemical and histological analyses of our mouse model of BTHS cardiomyopathy, giving new insights into the etiology of BTHS cardiomyopathy, and establishing the fidelity of our mouse model for future studies of BTHS cardiomyopathy.

Materials and Methods

Data Availability

The data that support the findings of this study are available from the corresponding author upon reasonable request.

Mouse models

C57BL/6 mice (strain code: 027) were purchased from Charles River Laboratories.—The Clustered Regularly Interspaced Short Palindromic Repeats (CRISPR) / CRISPR-associated 9 (Cas9) system was utilized to generate the *Taz* floxed allele with exons 5 to 10 of the mouse *Taz* gene flanked by two LoxP sites. Hemizygous *Taz* cKO male (*Taz*$^{F/Y}$; Cre+) mice were generated by crossing floxed *Taz* females to Xenopus laevis myosin light-chain 2 (*Xmlc2)*-Cre males, which have been widely used to ablate genes in cardiomyocytes from embryonic day (E)7.5 with no cardiac toxicity[26, 27]. The specificity of Xmlc2-Cre has been demonstrated utilizing ROSA26-tdTomato indicator

mice[27]. *Taz* cKO males survive to adulthood and were used to crossed with heterozygous floxed *Taz* females (*Taz*$^{F/F}$; Cre-) to generate hemizygous *Taz* cKO males (*Taz*$^{F/Y}$; Cre+) and homozygous *Taz* cKO females (*Taz*$^{F/F}$; Cre+), as well as Cre negative controls. PCR primer sequences for genotyping are listed in Table SII.

Additional details on the methods used in this study are provided in the Supplemental Methods.

Statistical Analyses

For data presented in bar plot format, the column's height corresponds to the mean, the error bar marks 95% CI, and the dots represent the individual measurements. Statistical analysis was performed using GraphPad Prism 8.0 (GraphPad Software), with a two-tailed Student's t test or two-way ANOVA for comparisons among groups. P values of less than 0.05 were considered statistically significant.

Results

Deletion of *Taz* in cardiomyocytes results in DCM

To investigate underlying molecular mechanisms by which *TAZ* deficiency leads to progression of cardiomyopathy, we generated a floxed *Taz* mouse line with exons 5–10 of the mouse *Taz* gene flanked by two LoxP sites (Figure 1A). We then generated cardiomyocyte-specific *Taz* knockout (cKO) mice by crossing floxed *Taz* mice with *Xmlc2*-Cre transgenic mice[26, 27]. We performed quantitative PCR (qRT-PCR) by utilizing primers outside of the floxed region to determine mRNA levels of *Taz* in cKO and control hearts. Results revealed that deletion of exons 5–10 caused mRNA decay in cKO hearts (Figure SIA). Western blot analysis on whole ventricle tissue lysates and adult cardiomyocytes further confirmed effective deletion of Taz in cKO hearts (Figure 1B–1E). We did not observe truncated Taz proteins in cKO hearts. QRT-PCR analysis revealed that loss of *Taz* did not result in increased transcription of the other two mammalian acyltransferase, acyl-CoA:lysocardiolipin acyltransferase-1 (ALCAT1) , or MLCL acyltransferase 1 (MLCLAT1) (Figure SIA).

Taz cKO mice were born at expected Mendelian ratios, 77% of which survived beyond 50-weeks of age (Figure 1F). Fewer than 5% of cKO mice displayed lethality between 1-week and 2-months of age, with significantly enlarged hearts (Figure 1G, SIB). At 4-months of age, hearts of surviving cKOs appeared to have a more rounded shape relative to control littermates (Figure 1G). Quantification of the height and width of ventricles revealed that the width of cKO ventricles was larger than that of control ventricles (Figure SIC), resulting in a decreased height/width ratio in mutants relative to controls (Figure SID). Histological analysis of surviving cKO mice at 4-months of age revealed dilated LV chambers when compared to controls, although no overtly enlarged hearts were observed (Figure 1G, Figure SIE). No significant differences were observed in RV chambers (Figure 1G, Figure SIE). Consistent with these observations, cardiac phenotypes of BTHS patients affect the LV but not the RV[2, 3] with only one report of biventricular disease[28]. A comprehensive time course of echocardiographic measurements revealed decreased LV systolic function (FS) in cKO

mice relative to littermate controls (Figure 1H–1I). Consistent with histological observations, the majority of cKO mice developed DCM at 4-months of age, as evidenced by significantly increased LVIDd and LVIDs (Figure 1J–1K). No significant differences were observed in ventricular weight to body weight (VW/BW) or VW to tibia length (VW/TL) ratios between cKOs and controls at either 2 or 4-months of age (Figure SIF–IG).

Because *TAZ* is an X-linked gene, BTHS occurs almost exclusively in males. In familial BTHS, female carriers are usually asymptomatic[1, 2, 10]. It is theoretically possible for a female to manifest symptoms of BTHS due to skewed X-inactivation. One female BTHS patient has been described, who has mosaicism for monosomy X chromosome with a *TAZ* mutation[29]. Thus, we also performed echocardiographic measurement in female *Taz* cKO and control mice. Our results revealed DCM phenotypes in female cKOs, compared to controls, that were similar to those observed in male cKOs (Table SI). To determine whether *Taz* cKO mice display cardiac arrhythmias, we performed surface electrocardiograms (ECGs) in cKO and control mice at 2-weeks, 2-months and 6-months of age. No arrhythmias were identified in cKO mice (Figure SII). Consistent with molecular evidence of cardiac remodeling, cardiac fetal gene markers atrial natriuretic factor (*Anf*), and B-type natriuretic peptide (*Bnp*) were significantly increased in cKO hearts at 2-months of age, prior to overt cardiac dysfunction, as previously observed in other models[30, 31] (Figure 1L). However, profibrotic genes collagen α1 types I (*Col1a1*) or III (*Col3a1*) were not increased in cKO hearts compared to controls, at either 2 or 4-months of age (Figure SIH). Consistent with this, Masson's trichrome staining or TUNEL staining showed no increase in cardiac fibrosis or cardiomyocytes apoptosis, respectively, in cKO hearts (Figure SI I–IJ). Taken together, these data demonstrated that loss of Taz in cardiomyocytes resulted in DCM and heart failure.

Loss of Taz in cardiomyocytes leads to abnormal CL metabolism

Due to the large variability in total CL levels in patients, MLCL/CL ratio has been established to diagnose BTHS[2, 11] as well as to evaluate BTHS models in research[18, 21–25]. To determine whether *Taz* cKO hearts exhibited CL defects similar to those observed in BTHS patients, we performed a full parameter analysis of CL profiles, including assessing levels of CL and MLCL, as well as the fatty acyl side-chain composition of CL in ventricular tissues isolated from cKOs and controls. We observed an approximately 50% reduction total CL levels in cKO hearts at both 2 and 4-months of age when compared to controls (Figure 2A). Consistent with findings in BTHS patients[11], levels of MLCL, as well as the further degradation product dilyso-CL (DLCL), were elevated in cKO hearts, while MLCL and DLCL levels were low in control hearts (Figure 2B–2C, SIIIA–IIID). Thus, MLCL/CL ratios increased about 50-fold in cKOs relative to controls (Figure 2D). Moreover, analyses of CL species revealed accumulation of CLs with shorter and/or more saturated acyl groups in cKOs (Figure 2E–2F). Conversely, loss of Taz reduced the amount of mature CL species with longer and more unsaturated acyl groups, including tetralinoleoyl-CL (72:8), which is the most predominant form of CL in the heart (Figure 2E–2F). The abnormal CL profile observed in *Taz* cKO hearts was representative of a key feature in BTHS patient samples[11].

We further examined the levels of the precursors and intermediate products of CL biosynthesis in *Taz* cKO and control hearts. As shown in Figure 2G–2H, the levels of total phosphatidic acid (PA) and phosphatidylglycerol (PG) were significantly increased in cKOs. In addition, although the total levels of phosphatidylethanolamine (PE) and phosphatidylcholine (PC) were not altered (Figure SIIIE–IIIF), the PC and PE species likely containing linoleic acid, such as PC(36:2) (likely PC(18:0/18:2)) and PE(36:2) (likely PE(18:0/18:2)), accumulated in cKOs compared to controls (Figure 2I–2J). Taken together, these results demonstrated that loss of Taz in cardiomyocytes impaired CL remodeling.

Taz-mediated CL remodeling is essential to maintain mitochondrial respiratory chain supercomplexes (RCS)

Taz-mediated CL remodeling has been suggested as critical for mitochondrial respiration in yeast and cultured cells[18, 32]. However, the role of Taz-mediated CL in mitochondrial respiration has not been studied in an *in vivo* BTHS mammalian model. We assessed mitochondrial respiration capacity in the presence of substrates for complex I (pyruvate/malate and palmitoyl carnitine/malate) or complex II (succinate/rotenone), in *Taz* cKO and control hearts at 2-months of age, prior to evident appearance of cardiac dysfunction. We found that cKO mitochondria displayed reduced state 3 and maximal respiratory rates for all 3 substrates (Figure 3A–3E), suggesting that loss of *Taz* impaired mitochondrial respiration capacity. We further measured the enzymatic activities of all four complexes from cKO and control hearts at 2-months of age. Results revealed that loss of Taz did not alter the enzymatic activities of each individual complex (Figure 3F). Glycolysis can be increased to compensate for decreased mitochondrial respiration[33]. However, we did not observe significant differences in lactate production between cKO and control hearts, suggesting that glycolysis was not increased (Figure SIV).

Mitochondria are a major source of ROS, a byproduct of mitochondrial electron transfer activity. Reduction in mitochondrial respiration capacity results in elevated ROS[34]. To determine whether loss of *Taz* resulted in increased ROS production in mitochondria, we measured ROS and mitochondrial superoxide. Results revealed that levels of ROS and superoxide were elevated in mitochondria isolated from cKO hearts at 2-months of age, compared to those from controls (Figure 3G–3J). However, we did not observe significant difference in mitochondrial membrane potential between cKO and control mitochondria (Figure SV), suggesting that elevated levels of ROS and superoxide were owing to reduction respiration capacity[34]. Taken together, these results demonstrated that loss of *Taz* perturbed mitochondrial function and increased ROS production.

To investigate molecular mechanism by which loss of Taz impaired mitochondrial function, we first examined protein levels of components of mitochondrial OXPHOS pathway. Consistent with findings from BTHS patient-derived fibroblasts[35] and iPSCs[32], protein levels of NDUFB8 (complex I), SDHA and SDHB (complex II), UQCRC2 and UQCRFS1 (complex III), MTCO1 and COX IV (complex IV), and ATP5A1 (complex V) were comparable between control and cKO hearts (Figure 4A–4B, SVI). The observation that there were no alterations in total protein levels of OXPHOS proteins, together with results that activities of individual complexes were not changed in cKO mitochondria (Figure 3F),

suggested that the decreased respiration rate in cKO mitochondria was not due to defects in each individual complex.

For efficient electron transport to occur, respiratory chain complexes must be organized into large oligomers of different composition and stoichiometry, referred as RCS[36]. RCS are formed by complex I, which builds a platform for binding of dimeric complex III (III_2) and several copies of complex IV[36]. Although it has been suggested that RCS are destabilized in BTHS patient-derived lymphoblasts[37], fibroblasts[35], and iPSCs[32], as well as in *Taz* knockouts in yeast[38], it is controversial as to whether *Taz* deficiency destabilizes individual complexes, low molecular weight heterooligomeric complexes, or RCS[32, 35, 37]. We next analyzed the structural organization of RCS in Taz cKO hearts at 2-months of age. Our results showed that higher-order assemblies of complexes I- and III-containing RCS were diminished in cKO mitochondria compared to controls (Figure 4C–4D, 4F–4G, 4I–4J). However, the lower molecular weight oligomers of RCS containing complexes I and III_2, as well as individual complexes I and III, were increased in cKO mitochondria (Figure 4C–4D, 4F–4G, 4I–4J). A significant reduction in complex IV-containing RCS was also observed in cKO mitochondria, while individual complex IV was accumulated (Figure 4E, 4H, 4K). Notably, rearrangements of RCS in mitochondria isolated from cKO hearts were consistent with those from BTHS patient-derived iPSCs[32]. Amounts of individual complexes II and V were not significantly different between cKO and control mitochondria (Figure 4E, 4L), likely because complexes II and V are excluded from supercomplexes[36]. These results suggest that TAZ-mediated CL remodeling is critical for the assembly of high order oligomers of RCS, which is essential for maintaining highly efficient electron transport[36].

Taz deficiency results in abnormal mitochondrial morphology and ultrastructure

Electron micrographs of cardiac muscle biopsies from BTHS patients have revealed mitochondrial malformations, including abnormal sizes, disorganized distribution, and tightly stacked or circular bundles of cristae[1]. However, detailed mechanisms underlying these abnormal mitochondrial structural features remain unclear. To assess the effect of loss of Taz on mitochondrial ultrastructure, we have performed TEM analysis on hearts isolated from *Taz* cKO and control mice at 2-months of age, selecting those mutants that did not yet show overt cardiac dysfunction at this age, thus making it less likely to observe alterations that occurred secondary to cardiac dysfunction. Overall, cKO hearts displayed a pronounced heterogeneity in mitochondrial morphology including variable sizes, abnormal shapes, and disorganized cristae structures, while sarcomere structure was not disturbed (Figure 5A–B). Intriguingly, in cKO hearts, we observed a significant number of mitochondria devoid of normal cristae structures, but with an increased inner membrane surface, forming large internal membrane stacks that failed to invaginate into tubular or fenestrated laminar cristae, which has been referred to as “onion-shaped” mitochondria (Figure 5B)[39].

To better evaluate the effect of loss of Taz on mitochondrial morphology and structure, we performed detailed quantification analysis of TEM images. Mitochondrial number was increased in cKO myocardium relative to controls (Figure 5C). An elevated number of abnormal mitochondria, including donut and onion shaped-mitochondria, as well as a remarkable number of mitochondria with disorganized cristae, in cKO hearts (Figure 5D).

Quantification of the mitochondrial area[40] showed a 50% reduction in cKOs (Figure 5E–G), while mitochondrial lengths were slightly increased in cKOs (Figure 5F–5H), suggesting that some mitochondria became elongated with a smaller cross-sectional area. We further applied a sphere fitting algorithm (refer to methods)[41, 42] within the mitochondrial area to determine the size and the shape of mitochondria in cKO and control hearts. Histograms of sphere radius distributions showed the typical normal distribution of spherical fitting size in controls, but a leftward shift and wider peak in cKOs, reflecting smaller mitochondria and more heterogeneity in mitochondrial shapes in cKO hearts (Figure 5I–5J).

Mitochondria are capable of modulating their shape and interorganelle connectivity by fusion or fission events[43]. Altered mitochondrial dynamics results in abnormal mitochondrial size and length. We examined proteins involved in mitochondrial fusion and fission in *Taz* cKO and control hearts. Results revealed that mitochondrial fusion proteins Mfn1 and Mfn2 were dramatically decreased, while the long isoform of Opa1 was slightly decreased, in cKO hearts compared to control hearts (Figure 6A, SVIIA). However, the mitochondrial fission protein Drp1 and its phosphorylation status were unaffected (Figure 6A, SVIIA). Notably, deletion of both Mfn1 and Mfn2 in adult cardiomyocytes results in smaller size but more mitochondria[44]. Taken together, our results demonstrated that Taz-mediated CL remodeling was critical to mitochondrial structure, morphology and dynamics.

Dysregulation of cristae formation pathways in *Taz* cKO hearts

Taz deficiency resulted in disorganized cristae structures, including “onion-shaped” cristae (Figure 5A–5B), typical manifestations of defects in cristae junction (CJ) formation and the architecture of cristae tips[39]. Multiple “cristae-shaping” proteins cooperatively control formation and maintenance of cristae[39]. The Mitochondrial Contact Site and Cristae-Organizing System (MICOS) is essential for CJ formation, while the assembly of dimeric and oligomeric F1F0-ATP synthase participates in forming and maintaining the typical convex curvature of cristae tips[39]. F1F0-ATP synthase subunit *e* (ATP5I) and subunit *g* (ATP5L) promote dimerization and oligomerization of F1F0-ATP synthase but are dispensable for ATP synthase monomer assembly or enzyme activity[39]. Abnormal mitochondrial morphologies in *Taz* cKO hearts are similar to those that occur when MICOS subunits are deleted or overexpressed[39], and to those observed in F1F0-ATP synthase Subunit *e/g* mutants[39], suggesting potential dysregulation of MICOS and/or F1F0-ATP synthase in *Taz* cKO hearts. To assess whether loss of *Taz* affected levels of MICOS, we examined levels of MICOS proteins in total lysates from cKO and control hearts at 2-months of age. Results revealed that protein levels of MIC60 and MIC25 were significantly increased in cKO hearts, while protein levels of MIC19, MIC10, MIC26, MIC27 or MIC13 were not changed (Figure 6B, SVIIB). To determine whether increased MICOS subunits were incorporated into MICOS complexes with other subunits, we analyzed MIC60 or MIC25 containing-MICOS complexes and found that levels of MIC60 or MIC25-containing complexes were increased in cKO hearts. Although protein levels of individual MIC19 or MIC10 subunits were not altered in cKO hearts, complexes containing these subunits were increased in cKO hearts, further demonstrating that levels of MICOS complexes were significantly increased in cKO mitochondria (Figure 6C, SVIIC–SVIIG).

MICOS proteins act in an antagonistic manner to F1F0-ATP synthase oligomers[39]. Overexpression of MIC60 leads to reduced levels of F1F0-ATP synthase oligomers, enlargement of cristae junction diameters and branching of cristae[39]. In *Taz* cKOs, in addition to onion-shaped structures, we observed hyperbranching of cristae (Figure 6B red arrow heads), previously described in yeast with F1F0-ATP synthase subunit *e* or *g* knocked out, or overexpressing MIC60[39]. We next analyzed protein levels of components of the F1F0-ATP synthase complex. We found that protein levels of subunits ATP5I and ATP5L were decreased, while ATP5A1 and ATP5F1 were not altered (Figure 6D, SVIIH). ATP5I and ATP5L control the dimerization and oligomerization of F1F0-ATP synthase[39]. We further examined the dimerization and oligomerization of the F1F0-ATP synthase complex. Results revealed that dimeric and oligomeric forms of F1F0-ATP synthase were decreased in cKO mitochondria, whereas monomeric forms were not affected (Figure 6E, SVII I–K). These results further delineated molecular mechanisms by which loss of Taz disrupted mitochondrial morphology and ultrastructure.

Discussion

Cardiac mitochondria occupy approximately one-third of the volume of adult cardiomyocytes, and provide over 90% of the ATP required for normal cardiac function[45–47]. Many essential mitochondrial functions are dependent on the mitochondrial-specific phospholipid CL[2]. Mutations in *TAZ* cause BTHS, a life-threatening disorder that disrupts the metabolism of CL[1, 2, 10]. Cardiomyopathy is the major clinical feature in BTHS[1, 2, 10]. However, an in-depth analysis of cardiac phenotype, specific lipid abnormalities, and mitochondrial form and function in an *in vivo* BTHS cardiomyopathy model are lacking. In the present study, we performed a detailed functional, biochemical and histological analyses of BTHS cardiomyopathy by utilizing a *Taz* cKO mouse model.

The cardiac defects in BTHS patients most frequently includes DCM, sometimes Left ventricular noncompaction and less often hypertrophic cardiomyopathy[1–3]. Additional cardiac issues include arrhythmia and fetal cardiomyopathy with or without intrauterine fetal demise[1–3]. Our *Taz* cKO mice displayed DCM phenotypes, while ventricular noncompaction and cardiac arrhythmia were not observed. The DCM phenotypes in cKO mice differ from those of previously described *Taz* knockdown mouse models, which show mild cardiac phenotypes[21–23] or striking cardiac dysfunction at embryonic and neonatal stages[24]. Analysis of a large group of animals showed some variability in cardiac phenotypes of cKO mice. A small cohort of cKO mice exhibited lethality between 1-week and 2-months of age, and displayed significantly enlarged hearts. The majority of cKO mice displayed DCM at 16-weeks of age, maintaining a relatively stable cardiac phenotype. This observation is consistent with the situation for BTHS patients. Those who survive infancy can live into their late forties with stabilized fractional shortening[1–3]. In recent decades, up to 70% of individuals with BTHS survive into adulthood[48], owing to improvements in disease diagnosis and management, including management of associated neutropenia/infectious risks, skeletal and cardiac myopathy[48, 49]. This emphasizes the importance and utility of a carefully characterized model of BTHS cardiomyopathy for testing therapies toward improved management of adult BTHS cardiomyopathy.

Taz mutation causes inefficient CL remodeling, resulting in a low total CL concentration, abnormal CL fatty acyl composition, and elevated MLCL/CL ratios in BTHS patients[11]. However, data quantifying distinct CL species and their fatty acyl side-chain composition in a TAZ deletion mouse model have been lacking. Our study provides a full parameter analysis of CL profiles, including levels of CL and MLCL, as well as assessing the fatty acyl side-chain composition of CL in a BTHS cardiomyopathy model. Consistent with BTHS patients, *Taz* cKO hearts displayed a typical BTHS CL profile, with low total CL concentration, abnormal CL fatty acyl composition, and elevated MLCL/CL ratios[11]. We observed a 50% reduction in CL and a 40% reduction in tetralinoleoyl-CL in cKO hearts. Residual CL and tetralinoleoyl-CL in cKO hearts could be due to the long half-life of CL[50], or to a contribution from non-cardiomyocytes. Moreover, we found accumulation of precursors and intermediate products in the CL biosynthesis pathway further demonstrating insufficient CL remodeling in cKO hearts. These data are informative for future studies of BTHS cardiomyopathy and CL function in heart by utilizing this *Taz* cKO mouse model.

Our studies are the first to analyze mitochondrial morphology in *Taz* cKO hearts at stages prior to overt cardiac dysfunction. In addition to overall mitochondrial morphological abnormalities, we found disorganized cristae structures including “onion-shaped” cristae in cKO hearts. We further discovered dysregulation of two important pathways involved in in cristae morphogenesis, MICOS and F1F0-ATP synthase complexes[39]. Detailed analyses of mitochondrial function have not previously been performed in a *Taz* cKO mouse model. Our results revealed that mitochondrial respiration capacity is decreased in cKO mitochondria. Additionally, although it has been suggested that mitochondrial RCS are destabilized in BTHS patient-derived lymphoblasts[37], fibroblasts[35] and iPSC[32], as well as in Taz knockouts in yeast[38], it is controversial as to whether Taz deficiency destabilizes individual complexes or low molecule weight heterooligomeric complexes. Our results revealed that heterooligomeric forms of complex I and III_2 were increased in cKO mitochondria, while amounts of high molecular weight RCS containing complex I, dimeric complex III and several copies of complex IV were significantly decreased, therefore strongly suggesting that loss of Taz and consequent CL abnormalities impair the bridging of complex IV to the supercomplexes.

In summary, our mouse model mirrors multiple physiological and biochemical aspects of BTHS cardiomyopathy. Moreover, results from mitochondria analysis in Taz cKO mice revealed key features of mitochondrial cardiomyopathies, demonstrating the essential function of CL remodeling in cardiac mitochondria and in the progression of cardiomyopathy. Taken together, our results give important insight into the underlying etiology of BTHS cardiomyopathy, and provide a framework for testing therapeutic approaches to BTHS cardiomyopathy, and/or other mitochondrial-related cardiomyopathies. Findings from our study demonstrate the critical function of CL in mitochondrial function and molecular mechanisms governing the architecture of cristae and cristae junctions in mitochondria. These finding will potentially impact our general understanding of the molecular basis of mitochondrial function and mitochondrial cardiomyopathies.

Supplementary Material

Refer to Web version on PubMed Central for supplementary material.

Acknowledgements

We thank Dr. Ying Jones at the UCSD Electron Microscopy Core for help with the TEM experiment.

Sources of Funding

XF and SME are supported by National Institutes of Health (NIH). ABG is supported by NIH R01HL138560 and R01HL132300.

Nonstandard Abbreviations and Acronyms

BTHS	Barth syndrome
TAZ	Tafazzin
CL	cardiolipin
cKO	cardiomyocyte-specific knockout
IMM	inner mitochondrial membrane
MLCL	monolyso-CL
LV	left ventricular
Xmlc2	Xenopus laevis myosin light-chain 2
MICOS	Mitochondrial Contact Site and Cristae-Organizing System
RCS	respiratory chain supercomplexes
TEM	transmission electron microscopy
OXPHOS	oxidative phosphorylation
TUNEL	Terminal deoxynucleotidyl transferase dUTP nick end labeling
LVIDd	end-diastolic LV internal diameter
LVIDs	end-systolic LV internal diameter
FS	percent fractional shortening
iPSCs	induced pluripotent stem cells

Reference

1. Barth PG, Scholte HR, Berden JA, Van der Klei-Van Moorsel JM, Luyt-Houwen IE, Van ‘t Veer-Korthof ET, Van der Harten JJ and Sobotka-Plojhar MA. An X-linked mitochondrial disease affecting cardiac muscle, skeletal muscle and neutrophil leucocytes. J Neurol Sci. 1983;62:327–55. [PubMed: 6142097]

2. Clarke SL, Bowron A, Gonzalez IL, Groves SJ, Newbury-Ecob R, Clayton N, Martin RP, Tsai-Goodman B, Garratt V, Ashworth M, et al. Barth syndrome. Orphanet J Rare Dis. 2013;8:23. [PubMed: 23398819]

3. Roberts AE, Nixon C, Steward CG, Gauvreau K, Maisenbacher M, Fletcher M, Geva J, Byrne BJ and Spencer CT. The Barth Syndrome Registry: distinguishing disease characteristics and growth data from a longitudinal study. Am J Med Genet A. 2012;158A:2726–32. [PubMed: 23045169]

4. Lesnefsky EJ, Slabe TJ, Stoll MS, Minkler PE and Hoppel CL. Myocardial ischemia selectively depletes cardiolipin in rabbit heart subsarcolemmal mitochondria. Am J Physiol Heart Circ Physiol. 2001;280:H2770–8. [PubMed: 11356635]

5. Paradies G, Petrosillo G, Pistolese M, Di Venosa N, Serena D and Ruggiero FM. Lipid peroxidation and alterations to oxidative metabolism in mitochondria isolated from rat heart subjected to ischemia and reperfusion. Free Radic Biol Med. 1999;27:42–50. [PubMed: 10443918]

6. Lesnefsky EJ, Chen Q, Slabe TJ, Stoll MS, Minkler PE, Hassan MO, Tandler B and Hoppel CL. Ischemia, rather than reperfusion, inhibits respiration through cytochrome oxidase in the isolated, perfused rabbit heart: role of cardiolipin. Am J Physiol Heart Circ Physiol. 2004;287:H258–67. [PubMed: 14988071]

7. Sparagna GC, Johnson CA, McCune SA, Moore RL and Murphy RC. Quantitation of cardiolipin molecular species in spontaneously hypertensive heart failure rats using electrospray ionization mass spectrometry. J Lipid Res. 2005;46:1196–204. [PubMed: 15772420]

8. O'Rourke B and Reibel DK. Effects of adrenoceptor blockade on cardiac hypertrophy and myocardial phospholipids. Proc Soc Exp Biol Med. 1992;200:95–100. [PubMed: 1349190]

9. Neuwald AF. Barth syndrome may be due to an acyltransferase deficiency. Curr Biol. 1997;7:R465–6. [PubMed: 9259571]

10. Bione S, D'Adamo P, Maestrini E, Gedeon AK, Bolhuis PA and Toniolo D. A novel X-linked gene, G4.5. is responsible for Barth syndrome. Nat Genet. 1996;12:385–9. [PubMed: 8630491]

11. Houtkooper RH, Rodenburg RJ, Thiels C, van Lenthe H, Stet F, Poll-The BT, Stone JE, Steward CG, Wanders RJ, Smeitink J, et al. Cardiolipin and monolysocardiolipin analysis in fibroblasts, lymphocytes, and tissues using high-performance liquid chromatography-mass spectrometry as a diagnostic test for Barth syndrome. Anal Biochem. 2009;387:230–7. [PubMed: 19454236]

12. Claypool SM, Whited K, Srijumnong S, Han X and Koehler CM. Barth syndrome mutations that cause tafazzin complex lability. J Cell Biol. 2011;192:447–62. [PubMed: 21300850]

13. Baile MG, Sathappa M, Lu YW, Pryce E, Whited K, McCaffery JM, Han X, Alder NN and Claypool SM. Unremodeled and remodeled cardiolipin are functionally indistinguishable in yeast. J Biol Chem. 2014;289:1768–78. [PubMed: 24285538]

14. Whited K, Baile MG, Currier P and Claypool SM. Seven functional classes of Barth syndrome mutation. Hum Mol Genet. 2013;22:483–92. [PubMed: 23100323]

15. Xu Y, Condell M, Plesken H, Edelman-Novemsky I, Ma J, Ren M and Schlame M. A Drosophila model of Barth syndrome. Proc Natl Acad Sci U S A. 2006;103:11584–8. [PubMed: 16855048]

16. Malhotra A, Edelman-Novemsky I, Xu Y, Plesken H, Ma J, Schlame M and Ren M. Role of calcium-independent phospholipase A2 in the pathogenesis of Barth syndrome. Proc Natl Acad Sci U S A. 2009;106:2337–41. [PubMed: 19164547]

17. Khuchua Z, Yue Z, Batts L and Strauss AW. A zebrafish model of human Barth syndrome reveals the essential role of tafazzin in cardiac development and function. Circ Res. 2006;99:201–8. [PubMed: 16794186]

18. Wang G, McCain ML, Yang L, He A, Pasqualini FS, Agarwal A, Yuan H, Jiang D, Zhang D, Zangi L, et al. Modeling the mitochondrial cardiomyopathy of Barth syndrome with induced pluripotent stem cell and heart-on-chip technologies. Nat Med. 2014;20:616–23. [PubMed: 24813252]

19. Schlame M, Kelley RI, Feigenbaum A, Towbin JA, Heerdt PM, Schieble T, Wanders RJ, DiMauro S and Blanck TJ. Phospholipid abnormalities in children with Barth syndrome. J Am Coll Cardiol. 2003;42:1994–9. [PubMed: 14662265]

20. Valianpour F, Wanders RJ, Barth PG, Overmars H and van Gennip AH. Quantitative and compositional study of cardiolipin in platelets by electrospray ionization mass spectrometry: application for the identification of Barth syndrome patients. Clin Chem. 2002;48:1390–7. [PubMed: 12194913]

21. Acehan D, Vaz F, Houtkooper RH, James J, Moore V, Tokunaga C, Kulik W, Wansapura J, Toth MJ, Strauss A, et al. Cardiac and skeletal muscle defects in a mouse model of human Barth syndrome. J Biol Chem. 2011;286:899–908. [PubMed: 21068380]
22. Soustek MS, Falk DJ, Mah CS, Toth MJ, Schlame M, Lewin AS and Byrne BJ. Characterization of a transgenic short hairpin RNA-induced murine model of Tafazzin deficiency. Hum Gene Ther. 2011;22:865–71. [PubMed: 21091282]
23. Huang Y, Powers C, Moore V, Schafer C, Ren M, Phoon CK, James JF, Glukhov AV, Javadov S, Vaz FM, et al. The PPAR pan-agonist bezafibrate ameliorates cardiomyopathy in a mouse model of Barth syndrome. Orphanet J Rare Dis. 2017;12:49. [PubMed: 28279226]
24. Phoon CK, Acehan D, Schlame M, Stokes DL, Edelman-Novemsky I, Yu D, Xu Y, Viswanathan N and Ren M. Tafazzin knockdown in mice leads to a developmental cardiomyopathy with early diastolic dysfunction preceding myocardial noncompaction. J Am Heart Assoc. 2012;1(2):jah3-e000455.
25. Wang S, Li Y, Xu Y, Ma Q, Lin Z, Schlame M, Bezzerides VJ, Strathdee D and Pu WT. AAV Gene Therapy Prevents and Reverses Heart Failure in A Murine Knockout Model of Barth Syndrome. Circ Res. 2020;126(8):1024–1039. [PubMed: 32146862]
26. Breckenridge R, Kotecha S, Towers N, Bennett M and Mohun T. Pan-myocardial expression of Cre recombinase throughout mouse development. Genesis. 2007;45:135–44. [PubMed: 17334998]
27. Liu C, Spinozzi S, Chen JY, Fang X, Feng W, Perkins G, Cattaneo P, Guimaraes-Camboa N, Dalton ND, Peterson KL, et al. Nexilin Is a New Component of Junctional Membrane Complexes Required for Cardiac T-Tubule Formation. Circulation. 2019;140:55–66. [PubMed: 30982350]
28. Hanke SP, Gardner AB, Lombardi JP, Manning PB, Nelson DP, Towbin JA, Jefferies JL and Lorts A. Left ventricular noncompaction cardiomyopathy in Barth syndrome: an example of an undulating cardiac phenotype necessitating mechanical circulatory support as a bridge to transplantation. Pediatr Cardiol. 2012;33:1430–4. [PubMed: 22427193]
29. Cosson L, Toutain A, Simard G, Kulik W, Matyas G, Guichet A, Blasco H, Maakaroun-Vermesse Z, Vaillant MC, Le Caignec C, et al. Barth syndrome in a female patient. Mol Genet Metab. 2012;106:115–20. [PubMed: 22410210]
30. Fan F, Duan Y, Yang F, Trexler C, Wang H, Huang L, Li Y, Tang H, Wang G, Fang X, et al. Deletion of heat shock protein 60 in adult mouse cardiomyocytes perturbs mitochondrial protein homeostasis and causes heart failure. Cell Death Differ. 2020;27:587–600. [PubMed: 31209364]
31. Fang X, Bogomolovas J, Wu T, Zhang W, Liu C, Veevers J, Stroud MJ, Zhang Z, Ma X, Mu Y, et al. Loss-of-function mutations in co-chaperone BAG3 destabilize small HSPs and cause cardiomyopathy. J Clin Invest. 2017;127:3189–3200. [PubMed: 28737513]
32. Dudek J, Cheng IF, Balleininger M, Vaz FM, Streckfuss-Bomeke K, Hubscher D, Vukotic M, Wanders RJ, Rehling P and Guan K. Cardiolipin deficiency affects respiratory chain function and organization in an induced pluripotent stem cell model of Barth syndrome. Stem Cell Res. 2013;11:806–19. [PubMed: 23792436]
33. Lee M and Yoon JH. Metabolic interplay between glycolysis and mitochondrial oxidation: The reverse Warburg effect and its therapeutic implication. World J Biol Chem. 2015;6:148–61. [PubMed: 26322173]
34. Aon MA, Cortassa S, Marban E and O'Rourke B. Synchronized whole cell oscillations in mitochondrial metabolism triggered by a local release of reactive oxygen species in cardiac myocytes. J Biol Chem. 2003;278:44735–44. [PubMed: 12930841]
35. Chatzispyrou IA, Guerrero-Castillo S, Held NM, Ruiter JPN, Denis SW, L IJ, Wanders RJ, van Weeghel M, Ferdinandusse S, Vaz FM, et al. Barth syndrome cells display widespread remodeling of mitochondrial complexes without affecting metabolic flux distribution. Biochim Biophys Acta Mol Basis Dis. 2018;1864:3650–3658. [PubMed: 30251684]
36. Gu J, Wu M, Guo R, Yan K, Lei J, Gao N and Yang M. The architecture of the mammalian respirasome. Nature. 2016;537:639–43. [PubMed: 27654917]
37. McKenzie M, Lazarou M, Thorburn DR and Ryan MT. Mitochondrial respiratory chain supercomplexes are destabilized in Barth Syndrome patients. J Mol Biol. 2006;361:462–9. [PubMed: 16857210]

38. Brandner K, Mick DU, Frazier AE, Taylor RD, Meisinger C and Rehling P. Taz1, an outer mitochondrial membrane protein, affects stability and assembly of inner membrane protein complexes: implications for Barth Syndrome. Mol Biol Cell. 2005;16:5202–14. [PubMed: 16135531]
39. Cogliati S, Enriquez JA and Scorrano L. Mitochondrial Cristae: Where Beauty Meets Functionality. Trends Biochem Sci. 2016;41:261–273. [PubMed: 26857402]
40. Berg S, Kutra D, Kroeger T, Straehle CN, Kausler BX, Haubold C, Schiegg M, Ales J, Beier T, Rudy M, et al. ilastik: interactive machine learning for (bio)image analysis. Nat Methods. 2019;16:1226–1232. [PubMed: 31570887]
41. Thovert JF, Yousefian F, Spanne P, Jacquin CG and Adler PM. Grain reconstruction of porous media: application to a low-porosity Fontainebleau sandstone. Phys Rev E Stat Nonlin Soft Matter Phys. 2001;63:061307. [PubMed: 11415092]
42. Mickel W, Munster S, Jawerth LM, Vader DA, Weitz DA, Sheppard AP, Mecke K, Fabry B and Schroder-Turk GE. Robust pore size analysis of filamentous networks from three-dimensional confocal microscopy. Biophys J. 2008;95:6072–80. [PubMed: 18835899]
43. Dorn G II. Mitochondrial fission/fusion and cardiomyopathy. Curr Opin Genet Dev. 2016;38:38–44. [PubMed: 27061490]
44. Chen Y, Liu Y and Dorn GW 2nd. Mitochondrial fusion is essential for organelle function and cardiac homeostasis. Circ Res. 2011;109:1327–31. [PubMed: 22052916]
45. Gustafsson AB and Gottlieb RA. Heart mitochondria: gates of life and death. Cardiovasc Res. 2008;77:334–43. [PubMed: 18006487]
46. Porter GA Jr., Hom J, Hoffman D, Quintanilla R, de Mesy Bentley K and Sheu SS. Bioenergetics, mitochondria, and cardiac myocyte differentiation. Prog Pediatr Cardiol. 2011;31:75–81. [PubMed: 21603067]
47. Zhou B and Tian R. Mitochondrial dysfunction in pathophysiology of heart failure. J Clin Invest. 2018;128:3716–3726. [PubMed: 30124471]
48. Rigaud C, Lebre AS, Touraine R, Beaupain B, Ottolenghi C, Chabli A, Ansquer H, Ozsahin H, Di Filippo S, De Lonlay P, et al. Natural history of Barth syndrome: a national cohort study of 22 patients. Orphanet J Rare Dis. 2013;8:70. [PubMed: 23656970]
49. Mazar I, Stokes J, Ollis S, Love E, Espensen A, Barth PG, Powers JH 3rd and Shields AL. Understanding the life experience of Barth syndrome from the perspective of adults: a qualitative one-on-one interview study. Orphanet J Rare Dis. 2019;14:243. [PubMed: 31699126]
50. Schlame M and Greenberg ML. Biosynthesis, remodeling and turnover of mitochondrial cardiolipin. Biochim Biophys Acta Mol Cell Biol Lipids. 2017;1862:3–7. [PubMed: 27556952]
51. Zhang Z, Mu Y, Veevers J, Peter AK, Manso AM, Bradford WH, Dalton ND, Peterson KL, Knowlton KU, Ross RS, et al. Postnatal Loss of Kindlin-2 Leads to Progressive Heart Failure. Circ Heart Fail. 2016; 9(8):10.1161/CIRCHEARTFAILURE.116.003129 e003129. [PubMed: 27502369]
52. Vaz FM, McDermott JH, Alders M, Wortmann SB, Kolker S, Pras-Raves ML, Vervaart MAT, van Lenthe H, Luyf ACM, Elfrink HL, et al. Mutations in PCYT2 disrupt etherlipid biosynthesis and cause a complex hereditary spastic paraplegia. Brain. 2019;142:3382–3397. [PubMed: 31637422]
53. Chambers MC, Maclean B, Burke R, Amodei D, Ruderman DL, Neumann S, Gatto L, Fischer B, Pratt B, Egertson J, et al. A cross-platform toolkit for mass spectrometry and proteomics. Nat Biotechnol. 2012;30:918–20. [PubMed: 23051804]
54. Fang X, Stroud MJ, Ouyang K, Fang L, Zhang J, Dalton ND, Gu Y, Wu T, Peterson KL, Huang HD, et al. Adipocyte-specific loss of PPARgamma attenuates cardiac hypertrophy. JCI Insight. 2016;1:e89908. [PubMed: 27734035]
55. Mu Y, Yu H, Wu T, Zhang J, Evans SM and Chen J. O-linked beta-N-acetylglucosamine transferase plays an essential role in heart development through regulating angiopoietin-1. PLoS Genet. 2020;16:e1008730. [PubMed: 32251422]
56. Woodall BP, Orogo AM, Najor RH, Cortez MQ, Moreno ER, Wang H, Divakaruni AS, Murphy AN and Gustafsson AB. Parkin does not prevent accelerated cardiac aging in mitochondrial DNA mutator mice. JCI Insight. 2019;5.

57. Pickles S, Arbour N and Vande Velde C. Immunodetection of outer membrane proteins by flow cytometry of isolated mitochondria. J Vis Exp. 2014:51887. [PubMed: 25285411]

58. Hou T, Zhang R, Jian C, Ding W, Wang Y, Ling S, Ma Q, Hu X, Cheng H and Wang X. NDUFAB1 confers cardio-protection by enhancing mitochondrial bioenergetics through coordination of respiratory complex and supercomplex assembly. Cell Res. 2019;29:754–766. [PubMed: 31366990]

59. Liang W, Moyzis AG, Lampert MA, Diao RY, Najor RH and Gustafsson AB. Aging is associated with a decline in Atg9b-mediated autophagosome formation and appearance of enlarged mitochondria in the heart. Aging Cell. 2020:e13187.

Clinical Perspective

What is new?

- A small fraction of Taz cKO mice exhibited lethality by two months of age, while the majority displayed ventricular dilation and compromised heart function at 4 months, remaining stable up to one year of age.
- Full parameter CL profiles were comparable to those of BTHS patients, including low total CL and abnormal acyl side chain composition.
- Mitochondrial analyses prior to overt cardiac dysfunction demonstrated impairment of complexes important for cristae morphogenesis, resulting in onion-shaped mitochondria, as seen in BTHS patient samples.
- Loss of Taz impairs the bridging of complex IV to supercomplexes, impairing respiration capacity in an *in vivo* model.

What are the clinical implications?

- Taz cKO mice display DCM with impaired but stable fractional shortening, consistent with recent findings in surviving BTHS patients.
- The lipid profile of Taz cKO hearts is comparable to that observed in BTHS patients.
- Mitochondrial malformations in Taz cKO hearts recapitulate features typical of those observed in cardiac biopsies from BTHS patients.
- Validation of the fidelity of the in vivo mouse model for studies of BTHS cardiomyopathy paves the way for our further understanding the etiology of BTHS cardiomyopathy, and for testing future therapies for BTHS cardiomyopathy and/or other mitochondrial-related cardiomyopathies.

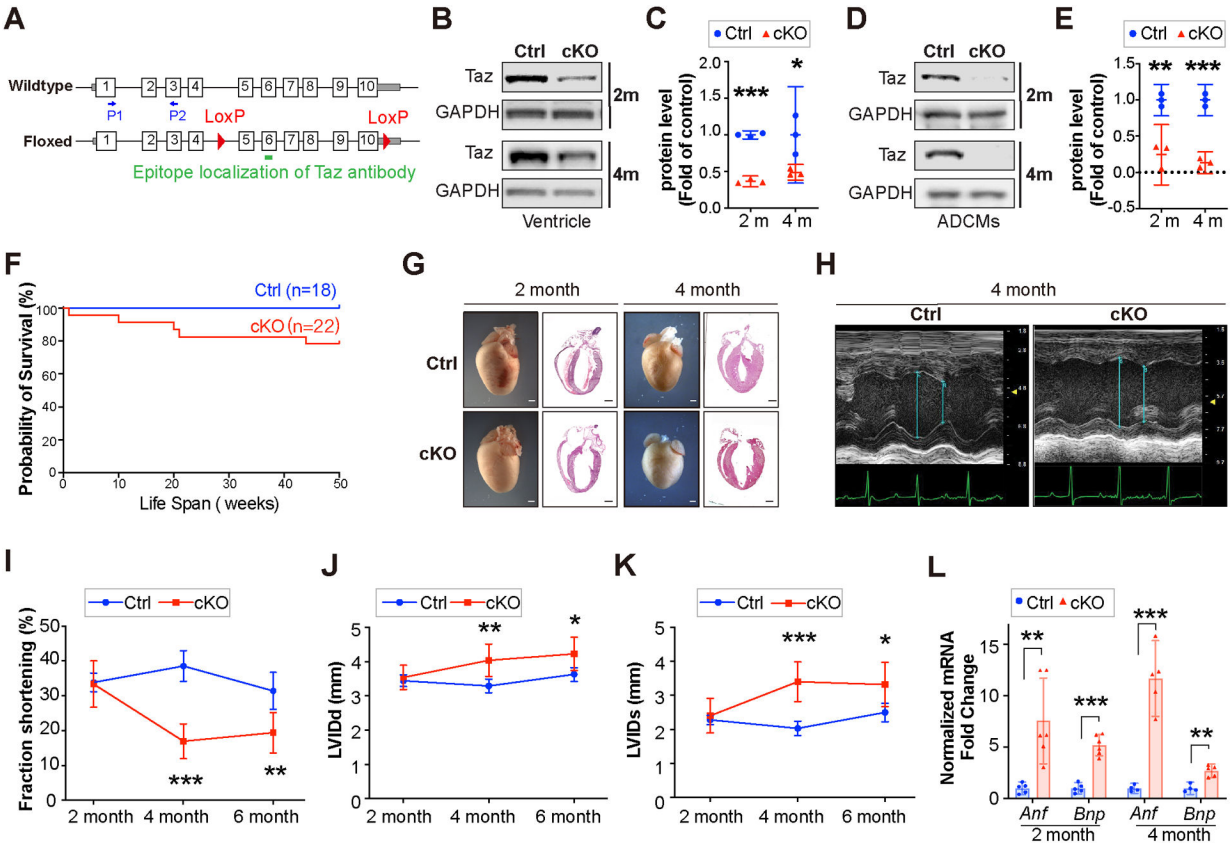

Figure 1. Deletion of Tafazzin (Taz) in cardiomyocytes resulted in dilated cardiomyopathy (DCM).

(A) Targeting strategy for the generation of *Tafazzin* (*Taz*) floxed mice. Two loxP sites (red) flanking exons 5–10 of *Taz* were inserted by utilizing CRISPR/Cas 9 technology. Gray box: 5'UTR and 3'UTR. The epitope localization of Taz antibody in exon 6 was indicated by green line. PCR primer sets for mRNA qRT-PCR genotyping are indicated by blue arrows. **(B-E)** Representative immunoblots (B and D) and quantification analysis (C and E) of Taz protein levels in whole ventricle tissue lysates and adult cardiomyocytes (ADCMs) isolated from *Taz* cardiomyocyte specific knockout (cKO) and control (Ctrl) mice at 2 and 4 months. GAPDH served as a loading control. n = 3 mice per group. **(F)** Kaplan-Meier survival curves for *Taz* cKO (n = 22) and control (Ctrl) (n = 18) mice. **(G)** Representative microscopic views of whole mouse hearts and four chamber-sectional views of Hematoxylin and Eosin (H&E)-stained sections from *Taz* cKO and Ctrl mice at 2 and 4 months of age. Scale bar: 1mm. **(H)** Representative echocardiographic images of *Taz* cKO and Ctrl mice at 4 months of age. **(I-K)** Echocardiographic measurements for Ctrl and cKO male mice (n = 7–10 mice at 2, 4, and 6 months of age) of (I) left ventricle (LV) FS (% FS), (J) LVIDd and (K) LVIDs. **(L)** Quantitative PCR (qRT-PCR) analysis of cardiac fetal gene markers, atrial natriuretic factor (*Anf*), and B-type natriuretic peptide (*Bnp*), in *Taz* cKO and Ctrl mouse hearts at 2 and 4 months of age. n = 5–6 mice per group. Data were normalized to corresponding 18S levels, and cKO is expressed as the fold-change versus control. *P < 0.05, **P < 0.01, ***P < 0.001, by a two-tailed Student's t test.

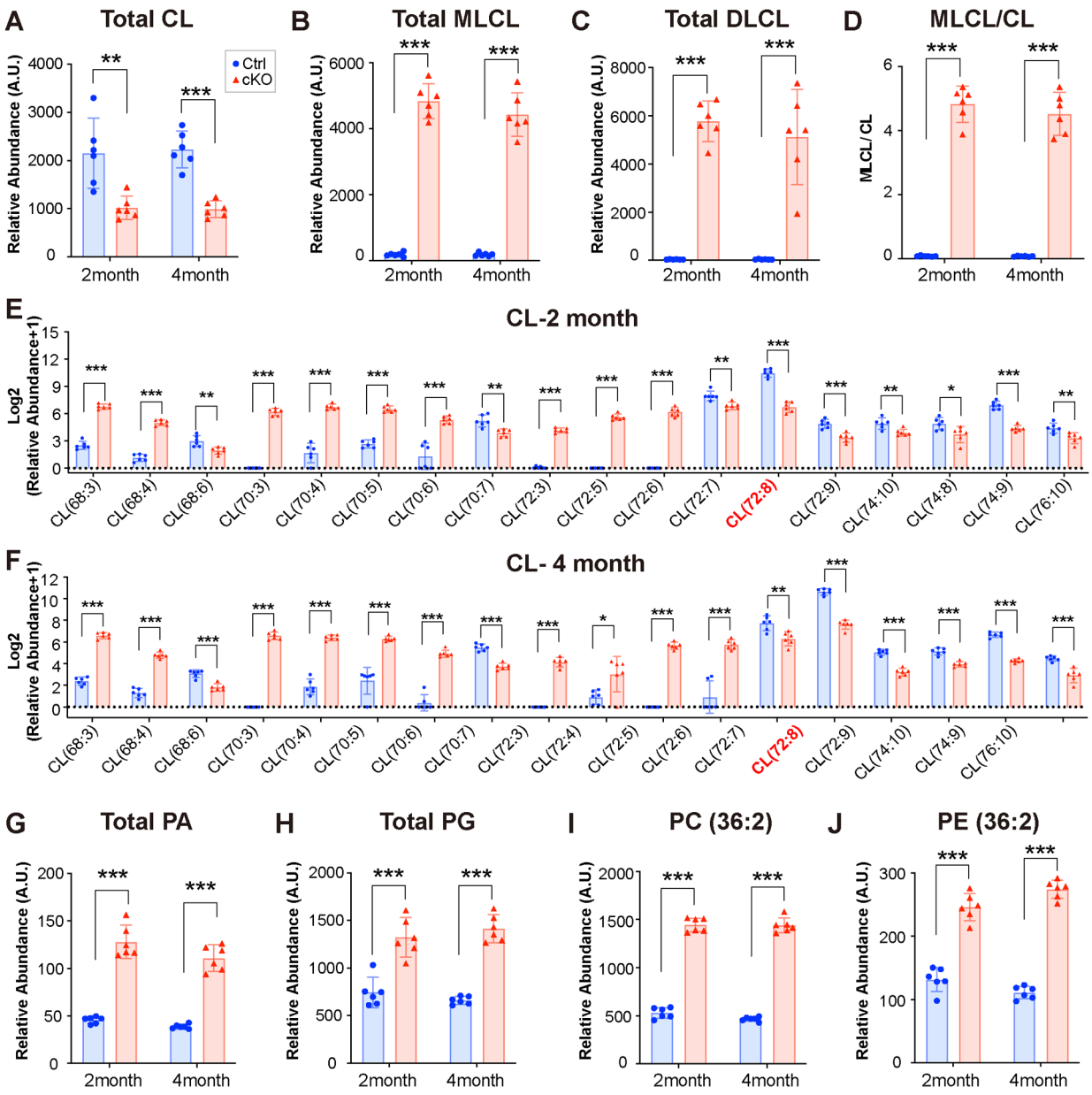

Figure 2. Loss of Taz in cardiomyocytes leads to abnormal cardiolipin (CL) metabolism.

(A-C) Levels of total CL (A), monolyso-CL (MLCL) (B), and dilyso-CL (DLCL) (C) in the ventricular tissues isolated from *Taz* cardiomyocyte-specific knockout (cKO) and control (Ctrl) mice at 2 and 4 months of age. **(D)** The ratio of MLCL to CL was calculated from the total MLCL and CL levels. **(E-F)** Levels of CL molecular species in the ventricle tissues isolated from *Taz* cKO and Ctrl mice at 2 months (E) and 4 months (F) of age. Red color highlighted the Tetralinoleoyl-CL molecule CL (72:8). **(G-J)** Levels of total phosphatidic acid (PA) (G), total phosphatidylglycerol (PG) (H), phosphatidylcholine (PC) (36:2) (I) and phosphatidyl ethanolamine (PE) (36:2) in the ventricular tissues isolated from *Taz* cKO and Ctrl mice at 2 and 4 months of age. n = 6 mice per group. *P < 0.05, **P < 0.01, ***P < 0.001, cKO versus Ctrl, by a two-tailed Student's t test.

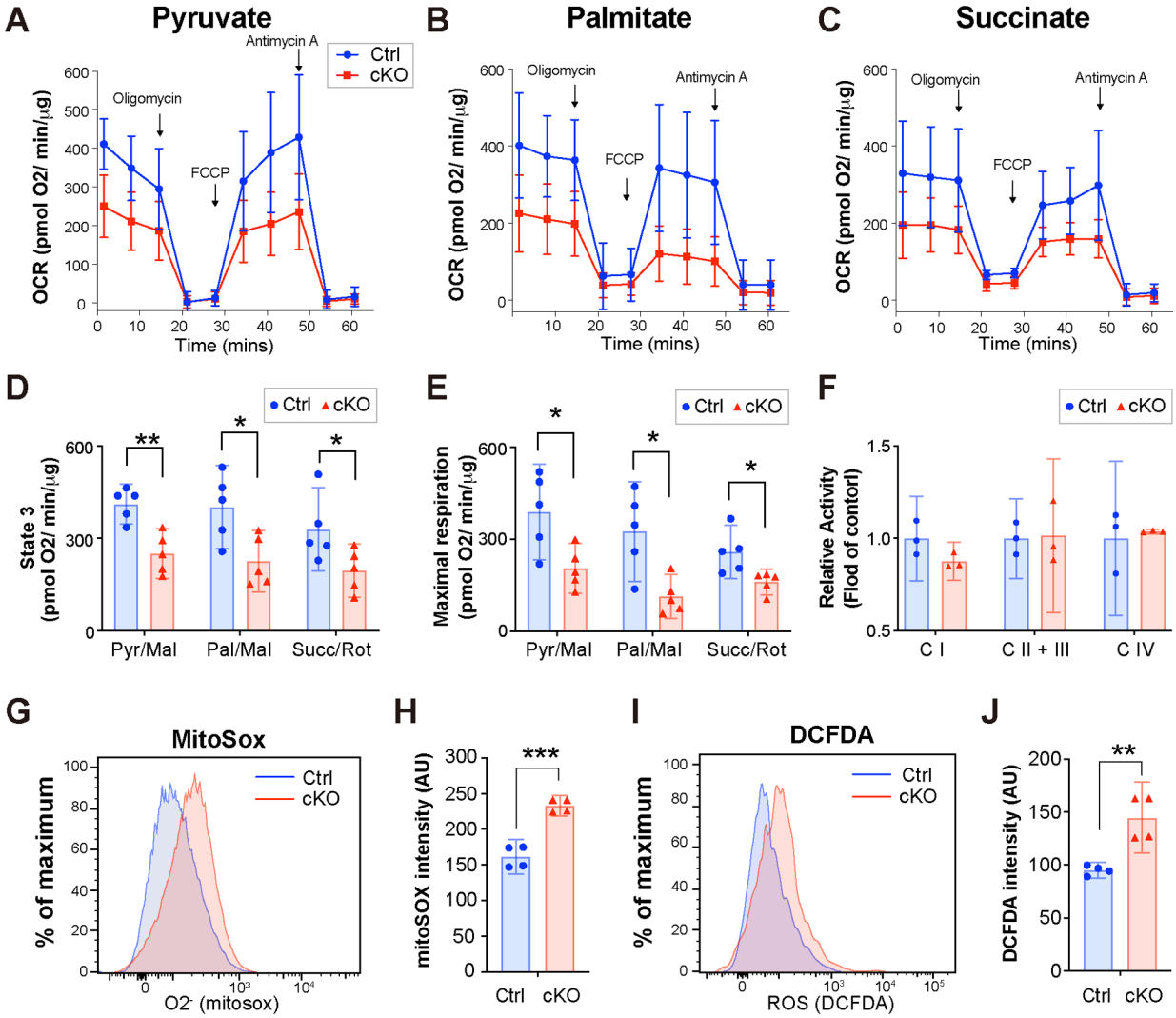

Figure 3. Mitochondrial functions are impaired in *Taz* cKO hearts at 2 months of age.

(A-C) Oxygen Consumption Rate (OCR) measurements for mitochondria isolated from *Taz* cKO (red) and control (Ctrl, blue) were obtained over time (min) using a Seahorse XF96 analyzer. Pyruvate/malate (A) and palmitate (B) were used for the substrates of complex I. Succinate/rotenone (C) was used for the substrates of complex II. n = 5 mice per group. **(D-E)** State 3 (ADP stimulated) (D) and maximal (FCCP uncoupled) (E) respiration rates of mitochondria were calculated from the measurements. Pyr/Mal, pyruvate/malate; Pal/Mal, palmitate/malate; Succ/Rot, succinate/rotenone. n = 5 mice per group. **(F)** Measurement of mitochondrial complex I, II, III, and IV enzymatic activities in freshly isolated mitochondria from *Taz* cKO (red) and control (Ctrl, blue) at 2 months. C, complex. n = 3 mice per group. **(G-J)** Representative FACS histograms (G and I) and quantified fluorescence intensity (H and J) of MitoSOX (G-H) and DCFDA (I-J) staining on the mitochondria isolated from *Taz* cKO (red) and control (Ctrl, blue) hearts at 2 months of age. n = 4 mice per group. *P < 0.05, **P < 0.01, ***P < 0.001, cKO versus Ctrl, by a two-tailed Student's t test.

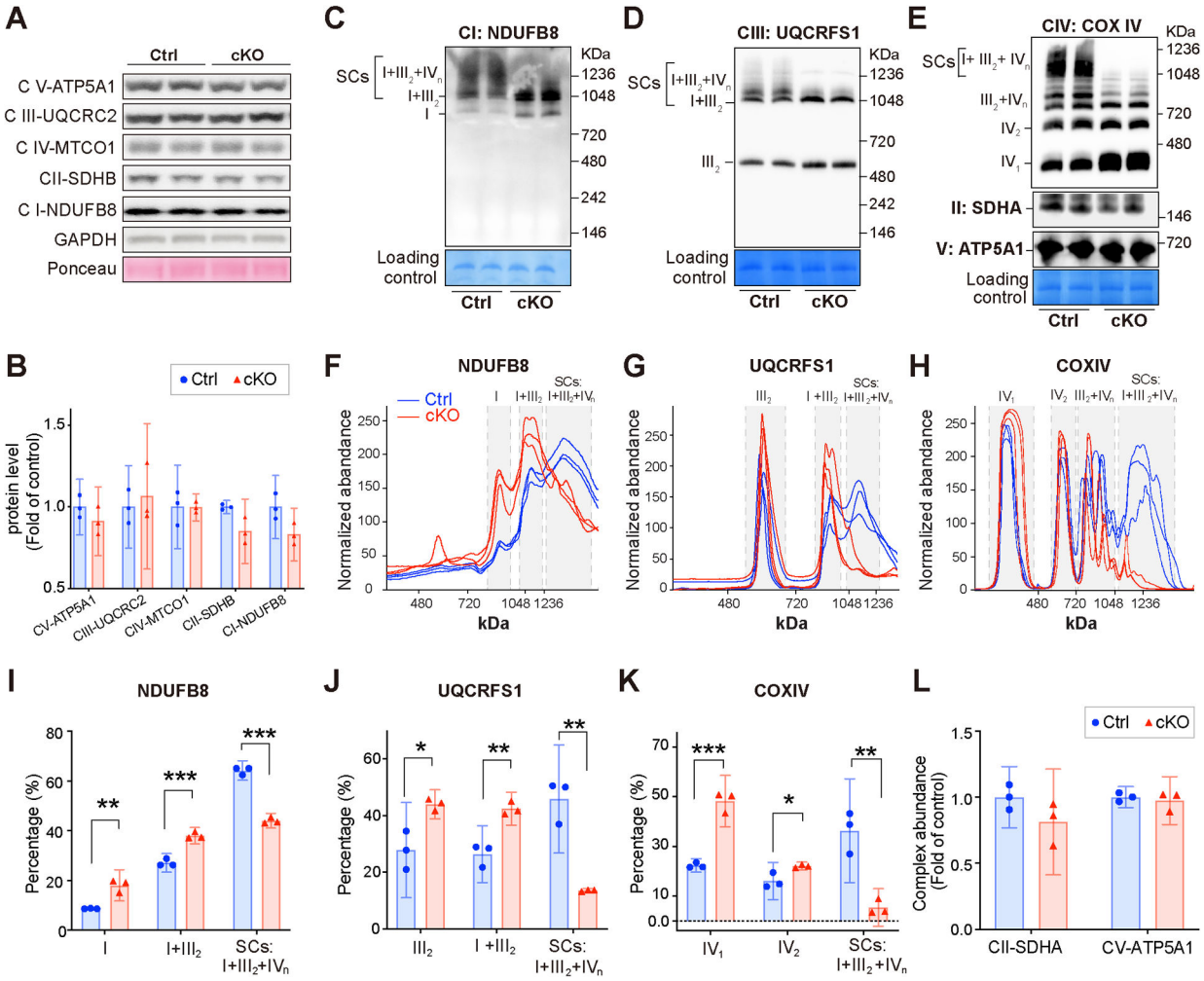

Figure 4. Taz is essential to maintain mitochondria respiratory chain supercomplexes (RCS).

(A-B) Representative western blots (A) and quantification analysis (B) of proteins involved in mitochondrial oxidative phosphorylation in total protein isolated *Taz* cKO and control (Ctrl) hearts at 2 months of age. C, Complex. GAPDH and Ponceau S (Ponc S) served as loading controls. n = 3 mice per group. **(C-H)** Representative image (C, D, E) and quantification analysis (F, G, H) of individual respiratory chain complexes and supercomplexes (SCs) analyzed by blue native (BN)-PAGE in *Taz* cKO and control (Ctrl) hearts at 2 months of age. Protein complexes were visualized by antibodies against subunits of complex I (CI, NDUFB8) (C, F), complex III (CIII, UQCRFS1) (D, G), and complex IV (CIV, COX IV) (E top, and H). Complex II was visualized by antibody against SDHA (E middle), and complex V with antibody against ATP5A1 (E bottom). Coomassie blue stained membranes were scanned for loading controls. n = 3 mice per group. **(I)** Percentages of NDUFB8 containing individual complex I, heterooligomeric form of complex I and III_2, and supercomplexes (SCs). **(J)** Percentages of UQCRFS1 containing individual complex III, heterooligomeric form of complex I and III_2, and supercomplexes (SCs). **(K)** Percentages of COX IV containing individual complex IV, heterooligomeric form of III_2 and IV, and supercomplexes (SCs). **(L)** Quantification analysis of individual respiratory chain complexes

II (SDHA) and V (ATP5A1). *P < 0.05, **P < 0.01, ***P < 0.001, cKO versus Ctrl, by a two-tailed Student's t test.

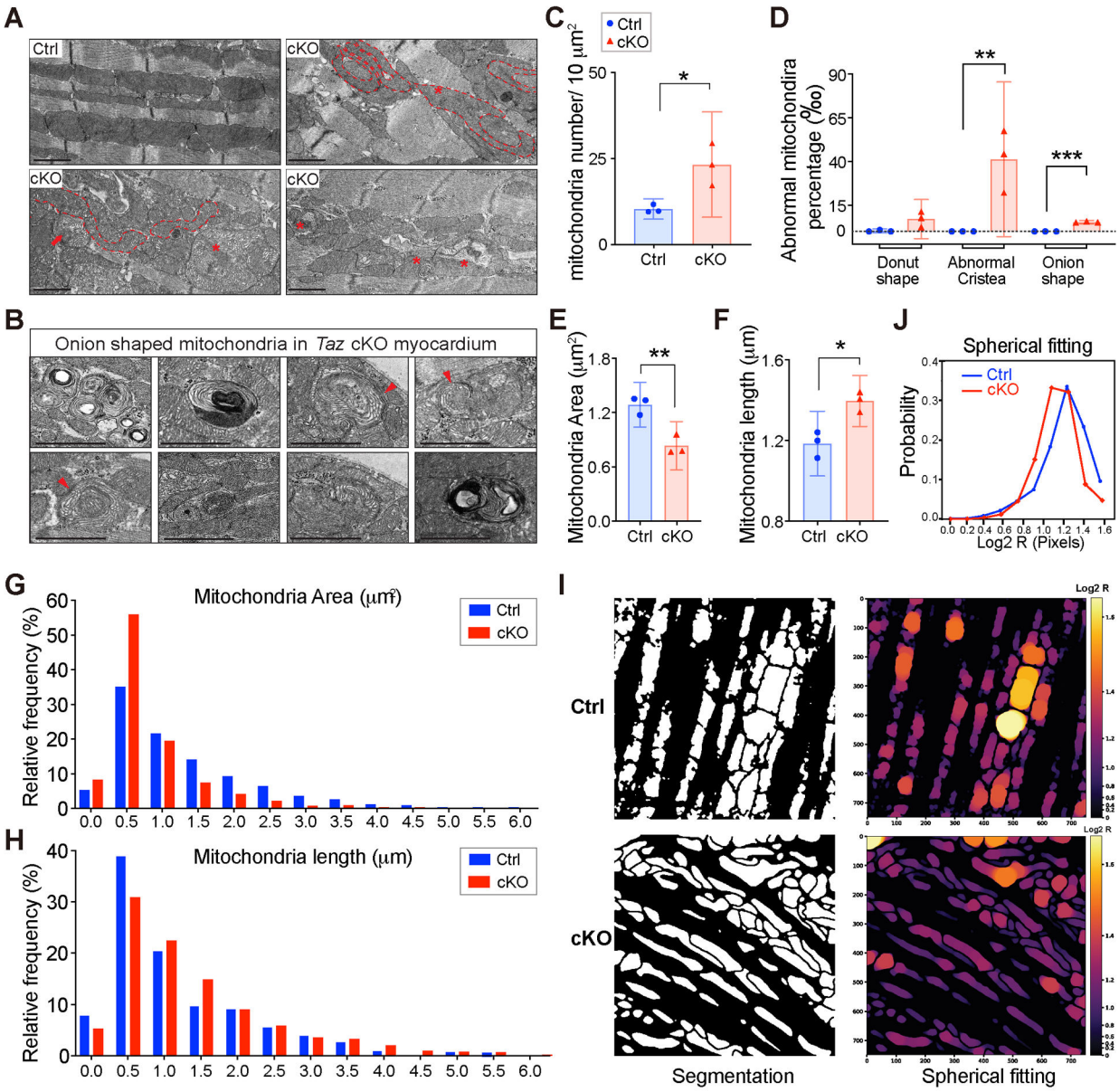

Figure 5. Taz deficiency causes morphology and ultrastructure defects.

(A) Representative electron micrographs of control (Ctrl) and *Taz* cKO hearts at 2 months of age showing abnormal mitochondrial morphology (red dashed lines) and disorganized inner mitochondrial membranes (red asterisks). The red arrow points to an “onion-shaped” mitochondrion. Scale bar: 1 μm. **(B)** Higher magnification views of **“**onion-shaped” mitochondria in *Taz* cKO hearts, with extensive cristae branching indicated by red arrowheads. Scale bar: 1 μm. **(C)** Quantification of mitochondria number per 10 μm^2 in control (Ctrl) and *Taz* cKO hearts at 2 months of age. **(D)** Quantification of the percentage of abnormal mitochondria in control (Ctrl) and *Taz* cKO hearts at 2 months of age. **(E-F)** Measurement of mitochondria size (E) and length (F) in control (Ctrl) and *Taz* cKO hearts at 2 months of age. **(G-H)** Quantification of mitochondrial size (G) and length (H) shown as frequency distributions, for which the bin center is indicated. **(I)** Representative

segmentation (left, white: mitochondria area; black: background) and spherical fitting (right) output. FireLUT indicates increasing sphere radius. Colorbar was scaled to log2R (Radius of sphere). **(J)** Quantification of sphere radius distribution were computed. X-axis labels was transformed with log2R. Blue curve indicated Ctrl mouse; red curve indicated *Taz* cKO mouse. n=2275 mitochondria from 3 control (Ctrl) mice and 2240 mitochondria from 3 *Taz* cKO mice. *P < 0.05, **P < 0.01, ***P < 0.001, cKO versus Ctrl, by a two-tailed Student's t test.

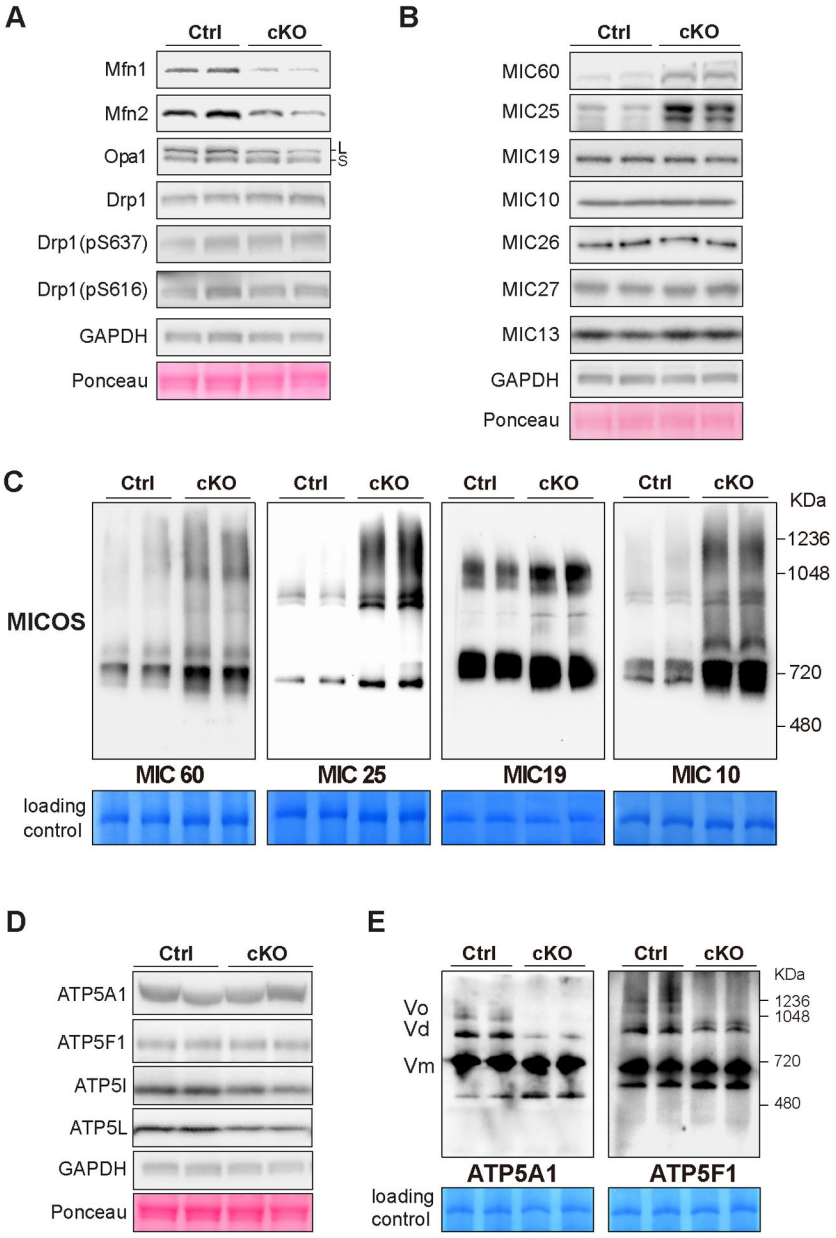

Figure 6. Loss of *Taz* causes dysregulation of pathways critical for mitochondrial cristae formation and dynamic.

(A) Representative western blots of Mfn1, Mfn2, Opa1, Drp1 and phosphorylated Drp1 (S637 and S616) in control (Ctrl) and *Taz* cKO hearts at 2 months of age. GAPDH and Ponceau S (Ponc S) served as loading controls. n = 3 mice per group. **(B)** Representative western blots of MICOS subunits MIC60, 25, 19, 10, 26, 27, and 13. GAPDH and Ponceau S (Ponc S) served as loading controls. n = 3 mice per group. **(C)** Blue native (BN)-PAGE analysis of MIC60, 25, 19, and 10 containing MICOS complex in control (Ctrl) and *Taz* cKO mitochondria at 2 months of age. Coomassie blue stained membranes were scanned for loading controls. n = 3 mice per group. **(D)** Representative western blots of ATP5A1, ATP5F1, ATP5I and ATP5L in control (Ctrl) and *Taz* cKO hearts at 2 months of age. GAPDH and Ponceau S (Ponc S) served as loading controls. n = 3 mice per group. **(E)** Blue

native (BN)-PAGE analysis of the monomeric, dimeric and oligomeric forms of F1F0-ATP synthase complex in control (Ctrl) and *Taz* cKO mitochondria at 2 months of age. Coomassie blue stained membranes were scanned for loading controls. n = 3 mice per group.